Spatiotemporal Distribution of Heatwave Hazards in Chinese Mainland for the Period 1990-2019

Enter authors here: Wei Wu [1, 2], Qingsheng Liu [1, 2, 3], He Li [1], and Chong Huang [1]

[1] State Key Laboratory of Resources and Environmental System, Institute of Geographic Sciences and Natural Resources Research, Chinese Academy of Sciences, Beijing 100101, China.

[2] University of Chinese Academy of Sciences, Beijing 100049, China.

[3] Jiangsu Center for Collaborative Innovation in Geographical Information Resource Development and Application, Nanjing 210023, China.

Corresponding author: Qingsheng Liu (liuqs@lreis.ac.cn);Chong Huang (huangch@lreis.ac.cn)

†Additional author notes should be indicated with symbols (current addresses, for example).

Key Points:

- The first comprehensive heatwave study with a spatial resolution 0.01° in China.
- Heatwave indicators in most China areas are increase
- Four categories divided by hazard and its slope and ten furnace cities of China are defined

Abstract

Heatwaves occurred frequently in summers, severely harming natural environment and human society. While a few long-term spatiotemporal heatwave studies have been conducted in China at the grid scale, their shortcomings involve discrete distribution and poor spatiotemporal continuity. We used daily data of 691 meteorological stations to obtain torridity index (TI) and heatwave index (HWI) datasets (0.01°), to evaluate the spatiotemporal distribution of heatwaves in Chinese mainland for 1990-2019. The results were as follows: (1) TI rose but with fluctuations. The largest increase occurred in North China in July. Areas with hazard levels of medium and above accounted for 22.16%, mainly in the eastern and southern provinces of China, South Tibet, East and South Xinjiang, and Chongqing. The hazard indicators in Chongqing and central Zhejiang were at especially high levels, which is concerning. (2) Average heatwave frequency, intensity, and duration reached relatively high levels of 6-8, 20-25, and 11-16, respectively, in East and South Xinjiang and Southeast Tibet. (3) The study areas were divided into four categories according to the spatiotemporal distribution of hazards. The "high hazard and rapidly increasing" and "low hazard and keep increasing" areas accounted for 8.71% and 41.33%, respectively. (4) The proportions of units with significantly increased average hazard (AH) at city and county levels were 57% and 68%, respectively. Jinhua, Zhengzhou, Nanchang, Wuhan, Shaoxing, Changsha, Shijiazhuang, Nanjing, Wuxi, and Changzhou accounted for the top 10 AH among the 49 first-tier, new first-tier, and second-tier cities. "Ten Furnaces" at the top of the provincial capitals were Zhengzhou, Nanchang, Wuhan, Changsha, Shijiazhuang, Nanjing, Hangzhou, Haikou, Chongqing, and Hefei. Suzhou's AH rose the fastest. While the strategy of west development and of revitalizing northeast China progressed, and the urbanization level and population aging of developed areas were further developed, the continuously increasing heatwave hazard should be fully considered.

Plain Language Summary

In the context of global warming, heatwaves occurred frequently in summers in Chinese mainland, severely harming human health and economic society. However, spatial and temporal distributions and changes of heatwave hazards of the region are inadequately quantified and relative high-resolution mapping. Here, we assess heatwave hazards based on heatwave index calculated by quality-controlled air temperature and relative humidity data, and heatwave

frequency-intensity-duration assessment model. We show that the heat degree rose but with fluctuations for the period 1990-2019, and changes differed in different regions. The largest increase occurred in North China in July. Heatwave became longer, more frequent and more intense in most areas, representing heatwave hazards were high level and continuous rising, especially in Chongqing, provinces in East China, Southwestern Tibet and Xinjiang, which needed concening. We also ranked the top ten provincial capitals called "Ten Furnaces" based on average hazards, and they are Zhengzhou, Nanchang, Wuhan, Changsha, Shijiazhuang, Nanjing, Hangzhou, Haikou, Chongqing, and Hefei.

Key Words： heatwave; hazard assessment; heatwave index; spatiotemporal distribution; Chinese mainland

1 Introduction

Global warming has led to the increasing frequency and intensity of extreme climate disasters (IPCC, 2021; Suarez-Gutierrez et al., 2020), and heatwaves account for the highest mortality rate among all extreme disasters (Borden & Cutter, 2008; Pengelly et al., 2007). The 2003 European heatwave caused approximately 70,000 deaths (Armstrong et al., 2019; Mitchell et al., 2016; Suarez-Gutierrez et al., 2020), and at least 5758 heat-related deaths were caused by the 2013 Chinese heatwave (Gu et al., 2016; Kotharkar & Ghosh, 2021a; Luo & Lau, 2018). The 2019 Indo-Pakistani heatwave caused at least 400 deaths, accompanied by widespread drought and water scarcity (Kotharkar & Ghosh, 2021b), and was one of the factors that led to the Bihar encephalitis outbreak(Chatterjee, 2019). Furthermore, the 2021 heatwave in Western North America led to a record temperature of 49.6°C in Canada (World Weather Attribution, 2021), resulting in more than 1,400 deaths (Lin et al., 2022; Silberner, 2021). Therefore, research on heatwaves is imperative in the context of global warming.

A heatwave is a weather process involving high temperatures, high humidity levels, and a long duration, which leads to bodily discomfort and may threaten public health and safety, increase energy consumption, and affect social production activities (Grade of the Heat Wave, 2012). At present, various temperature indices are available to define heatwaves, such as air temperature (KNMI, 2020; Met Office, 2017; SMHI, 2020), surface temperature (Y. Liu & Quan, 2014), and dew point temperature (Alduchov & Eskridge, 1996); dew point temperatures are relevant due to high correlations with air temperature. There is a growing tendency to analyze

heatwaves using apparent temperature indices such as physiological equivalent temperature (PET) (China Meteorological Administration, 2013), standard effective temperature (SET) (Zare et al., 2018), temperature-humidity-wind index (THW) (Steadman, 1984), humidex (Masterton et al., 1979), wet-bulb globe temperature (WBGT) (Yaglou & Minaed, 1957), universal thermal climate index (UTCI) (Dong et al., 2020; Emmanuel, 2005), and heat index (HI) (Z. Huang et al., 2011), which take into consideration additional indicators such as relative humidity, wind speed, and atmospheric precipitation. Notably, no consistent definition exists regarding the temperature threshold and the number of days of a heatwave (Anderson & Bell, 2011). Previous studies have shown that there are differences in how populations in different regions adapt to climate (Bobb et al., 2014; K. Chen et al., 2015; Song et al., 2017; Yan et al., 2022), which means that it is rather unreasonable to judge a heatwave in a complex climate region based on a single absolute threshold or a simple relative temperature threshold.

In the Special Report on Managing the Risks of Extreme Events and Disasters to Advance Climate Change Adaptation(IPCC, 2012) and the Fifth Assessment Report (AR5) (IPCC, 2014) of the Intergovernmental Panel on Climate Change (IPCC), a risk-centered assessment framework was presented, in which risk was expressed as a function of hazard, exposure, and vulnerability (Estoque et al., 2020). Therefore, clarifying the spatiotemporal distribution of heatwave hazards is a necessary prerequisite for judging the evolutionary trend of heatwave risks. In the given framework, hazard was defined as the external factors of a system that pose a serious threat to the system (Wu et al., 2019). Some researchers have directly used the temperature index to define hazards (Dong et al., 2020; Estoque et al., 2020); however, the scientific literature shows that a heatwave hazard is a measure of the severity of heatwave events, usually determined by the intensity, duration, frequency, and extent of heatwaves (Anderson & Bell, 2011; Kang & Eltahir, 2018; Raei et al., 2018; Savić et al., 2018; S. Wang, 2021; Yao & Wang, 2021; Yin et al., 2020) and calculated using the graphic overlay method (Dai, Liu, Huang, et al., 2021; Dai, Liu, Wu, et al., 2021; Ian L. McHarg, 1969; Wu et al., 2022).

China is a sensitive and significant area for the impact of global climate change (Beijing Climate Center, 2021). Since the 21st century, heatwaves have frequently occurred in China, and heatwaves are expected to form the new normal of the country's summer weather in 2030 (Y. Ding, 2018). In addition, the results of Sun's (2018) study on Chinese heatwaves showed a linear increase in intensity and a significant increase in frequency. Early studies involving heatwave

hazard assessments in China used different definitions based on the meteorological stations considered and focused on small areas and short time periods, resulting in the shortcomings of discrete distribution and poor spatiotemporal continuity. For instance, Zhao et al. (2022) used the weighted average of surface temperature, air temperature, and air pressure to assess the hazard level in Ningxia for the years 2014–2019. Wang (2021) defined heatwave hazards based on the interpolated data of meteorological stations; duration, intensity, accumulated heat days, and the length and intensity of the return period were used to analyze the heatwave hazard level of the Yangtze River Delta region. Zhan et al.(2019) used 35℃ as the temperature for a heatwave and analyzed the heatwave characteristics, such as intensity and duration, of the North China Plain on a 0.5° grid scale interpolated by maximum temperature data. Relatively few long-term studies of Chinese heatwave hazards have been conducted with a finer grid unit scale and without the use of relative heat thresholds.

Since the 21st century, the intensity and extent of Chinese heatwaves have continued to increase, causing serious impacts on residents. For the present study, heatwaves were defined based on a heatwave index (HWI) calculated using the torridity index (TI) and heat index (HI), and an annual heatwave hazard dataset with a spatial resolution of 0.01° was built based on the daily monitoring data of 691 meteorological stations from May to September 1990–2019 in the Chinese mainland (hereinafter referred to as China). The spatiotemporal distribution of heatwave hazards in China was further evaluated for this period, and the average hazard (AH) trends at the city and county levels were determined.

2 Materials and Methods

2.1 Definitions of HWI and heatwaves

The heat index (HI) uses the relative and absolute thresholds to define a heat day, and considers the cumulative effect of adjacent days' TI. The results of previous study showed that HI is a valid index for predicting heatwave weather (Z. Huang et al., 2011); therefore, we used HI to identify and define the heatwave index (HWI) and heatwaves.

TI is similar to apparent temperature indices, while HI considers the cumulative effect of a heatwave. Considering the long durations of high-temperature heatwaves, in this study, the HWI of a heatwave was defined as the average value of the daily HI, and a heatwave was

defined as an event with TI ⩾ TI' for three consecutive days or more and HWI ⩾ 2.8; the HWI threshold was based on a comprehensive HI finding, indicating that the heat grade of the day reaches the heatwave standard if HI ⩾ 2.8. The calculation model is given below.

$$\begin{cases} TI=1.8\times MT-0.55\times(1.8\times MT-26)\times(1-0.6)+32, RH\leq 60\% \\ TI=1.8\times MT-0.55\times(1.8\times MT-26)\times(1-RH)+32, RH>60\% \end{cases} \quad (1)$$

$$HI=1.2\times\left(TI-TI^{'}\right)+0.35\sum_{i=1}^{N}1/nd_i\left(TI_i-TI^{'}\right)+0.15\sum_{i=1}^{N-1}1/nd_i+1 \quad (2)$$

$$HWI=\sum_{i=1}^{N}HI_i \quad (3)$$

TI' is the threshold of TI; TI_i represents TI of the i-th day before the current day; nd_i represents the number of days from the i-th day before the current day to the current day; HI_i represents the i-th day in a heatwave event; N represents the duration of the heatwave event, and the unit is day (d).

TI' was calculated from the quantiles of TI. First, samples (MT and RH) with MT > 33°C were selected from the daily meteorological data, and the TI sequence of samples was arranged in ascending order. The 50th quantile was selected as the local TI'. The calculation method is given below:

$$\begin{cases} \widehat{Q}_i(p)=(1-\gamma)X_{(j)}+\gamma X_{(j+1)} \\ j=int(p\times n+(1+p)/3) \\ \gamma=p\times n+(1+p)/3-j \end{cases} \quad (4)$$

Here, $\widehat{Q}_i(p)$ is the i-th quantile value; X is the TI sequence in ascending order;p is the quantile (0.50); n represents the total number of sequences; and j is the j-th sequence number.

First, daily TI raster datasets were determined based on the interpolated MT and RH, and then the TI' raster was calculated based on equation (4). Following this, TI' was used as the comparison data, and each TI was traversed. The obtained value was compared with the value at the corresponding pixel in the comparison data; a pixel value greater than the comparison data indicated heat and was marked as 1, while the opposite was marked as 0, resulting in a daily raster dataset of 0 and 1, for a total of 4590. The HI dataset was calculated based on the judgment dataset. According to the definition of a heatwave, the pixels with a single heat event (without interruption) comprising less than three heat days or HWI < 2.8 were ignored to obtain the HWI dataset; thus, the pixels in the heatwave represented the HWI of the heatwave, the

corresponding pixel of a single day with the highest HI in a single heatwave was marked as the HI of that day, and the pixel marked as 0 represented no heatwave occurrence.

2.2 Heatwave hazard assessment and classification

A heatwave hazard is usually defined based on the heatwave frequency, intensity, and duration. In this study, heatwave frequency (HWF), maximum HI of a heatwave (HWMHI), and maximum heatwave duration (HWMD) in a year—representing frequency, intensity, and duration, respectively—were used to calculate the heatwave hazard. To make the hazard values comparable from year to year, we calculated the maximum value of each indicator for the 30-year period, used this value to normalize the data, and then added the indicators with equal weight, as given in Equation (5):

$$\text{Hazard}=(\overline{\text{HWF}}+\overline{\text{HWMD}}+\overline{\text{HWMHI}})/3 \quad (5)$$

Based on the HWI dataset, the data were calculated separately for each year and for each pixel. The heatwaves were judged day by day, and the HWF value was increased by 1 in the case of a consecutive heatwave. If there was no value for HWMHI, the maximum value in this heatwave was assigned to HWMHI. If a value already existed, the new HWMHI value was compared with the existing value, and it was used if it was greater than the existing value. If there was no value for HWMD, the number of days for which the heatwave lasted was assigned to HWMD; if a value already existed, it was compared with the new value and replaced with the new value if the latter was greater than the existing value. This process was followed to obtain the HWF, HWMHI, and HWMD datasets for each year.

The natural breaks method was used to classify the spatial distribution and temporal trends of the average hazard (AH) values, and each was categorized as high, medium high, middle, medium low, or low (red section in Figure 2) and increasing, slightly increased, basically unchanged, slightly decreased, or decreased (green section in Figure 2). Apart from the above two classifications, the hazards in China were further divided into four categories: high hazard and rapidly increasing, high hazard and slightly decreased or no significant change, low hazard and keeps increasing, and others (blue section in Figure 2). Figure 2 presents the classification standards. In the spatiotemporal classification of hazards, an "or" relationship was present between bands of the same color section and an "and" relationship between bands of different color sections; for example, the "high hazard and rapidly increasing" category consisted of the

following four scenarios: high hazard and increased, high hazard and slightly increased, medium high hazard and increased, and medium high hazard and slightly increased.

The AH values were used to rank heatwave hazards in the Chinese administrative divisions, and the zoning statistics methodology was used in this study. We first obtained the AH means of each administrative division for the 30-year period and then ran a linear regression over time for each administrative region. Following this, we selected first-tier, new first-tier, and second-tier cities and counties and ranked them in descending order of AH and slope.

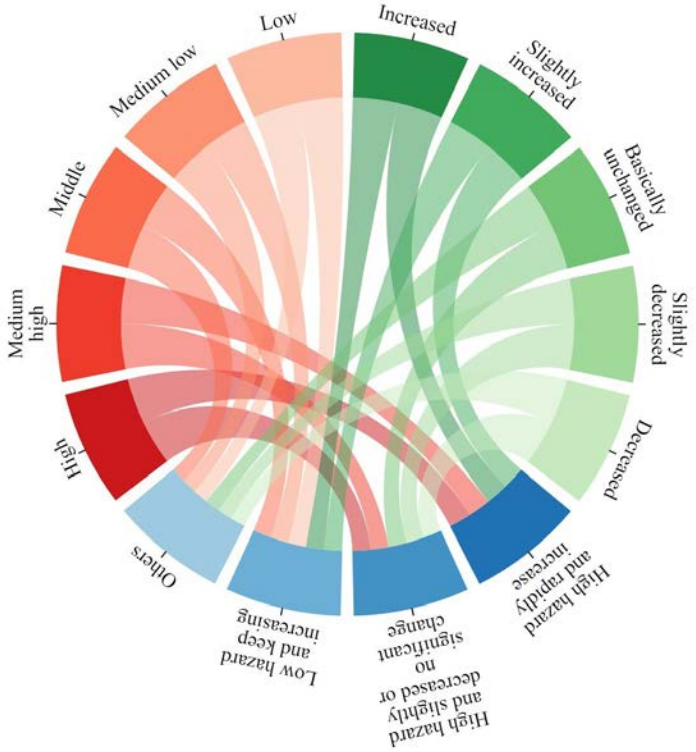

Figure 1. The standard for spatiotemporal classifications of heatwave hazards; the red and green sections represent the spatial distribution and temporal change classifications of heatwave hazards, respectively, and the blue section represents the spatiotemporal classifications of heatwave hazards

2.3 Analysis of the relative change of indicators

A time period spanning 30 years was chosen for this study. To better compare the changes in different indicators, the average values for the first five years (FY, 1990–1994) and the last five years (LY, 2015–2019) were considered. In addition, the level of change in each

indicator was different for each geographical division; for average TI (ATI), the change also differed each month. Therefore, ATI was analyzed in terms of the different geographical divisions and months, and each heatwave indicator was analyzed according to the different geographical partitions; then, the average values for FY and LY were calculated. Moreover, the concept of relative change (RC) was introduced to avoid the one-sidedness of the absolute change amount when comparing different months or divisions. RC was calculated as follows:

$$RC_{i,g(,m)}=(\overline{i_{LY,g(,m)}}-\overline{i_{FY,g(,m)}})/\overline{i_{g(,m)}} \quad (6)$$

Here, i, g, and m represent the different indicators (ATI, HWF, HWMHI, HWMD), different geographical divisions (N, NW, NE, SW, S, E), and different months (May, June, July, August, September), respectively; $\overline{i_{LY,g(,m)}}$和$\overline{i_{FY,g(,m)}}$represent the average value of LY and FY for an indicator; and $\overline{i_{g(,m)}}$ represents the average indicator value for the period 1990–2019. $RC_{i,g(,m)}>0.8$ meant that the indicator increased sharply for the geographical zone considered in a specific month (if RC was calculated).

3 Study area and Data

3.1 Study area

Spanning almost 50 degrees in latitude, China has a wide variety of climate types. Summer temperatures are consistently high across the country, and temperatures gradually decrease when the latitude increases. Generally speaking, summer in China spans the months June–August; however, in some cities and regions, temperature remains high in May and September, affecting a large number of people (T. Ding et al., 2010; He, Zhao, et al., 2022; A. Wang et al., 2022).

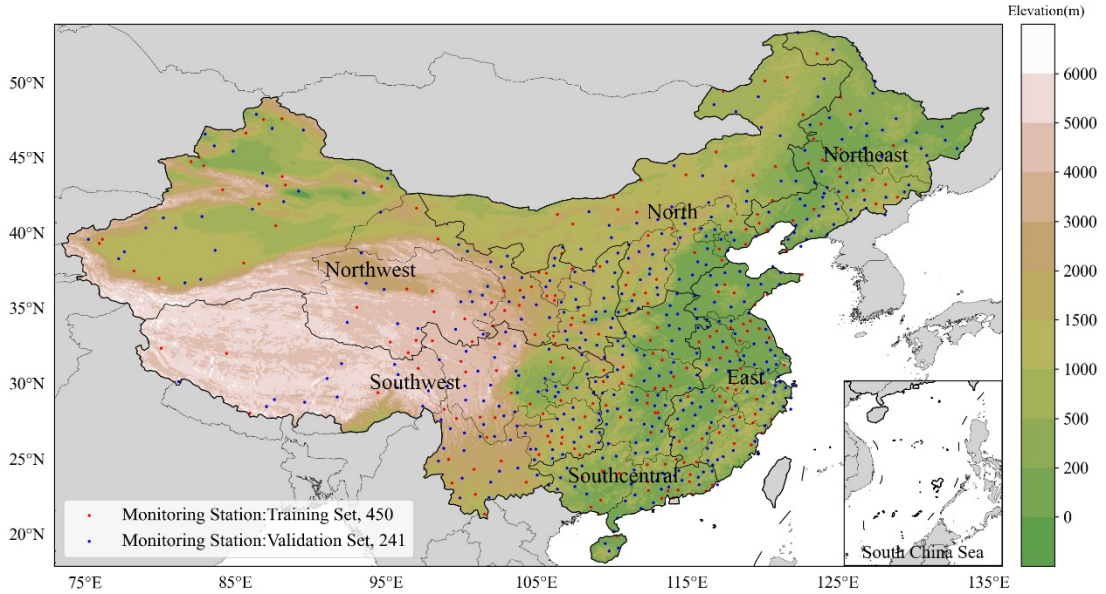

Figure 2. Domains of six geographical divisions—North (N), which consists of Beijing, Tianjin, Hebei, Shanxi, and Inner Mongolia; Northwest (NW), which consists of Xinjiang, Qinghai, Gansu, Ningxia, and Shaanxi; Northeast (NE), which consists of Heilongjiang, Jilin, and Liaoning; Southwest (SW), which consists of Tibet, Yunnan, Sichuan, Chongqing, and Guizhou; Southcentral (SC), which consists of Henan, Hubei, Hunan, Guangdong, and Guangxi; and East (E), which consists of Shandong, Anhui, Jiangsu, Shanghai, Zhejiang, Jiangxi, and Fujian—and meteorological stations (Four sets of random validation stations were selected to make their distribution more uniform. Containing of 10% of all stations, a total of 69, each set randomly selects one day of the month to apply, so a total of four days per month using only interpolation points for interpolation.)

2.2 Data sources

Maximum temperature (MT,°C) and average relative humidity (RH, %) data from 699 meteorological stations in China (Figure 1) for the years 1990–2019 were used to calculate the TI and HI; these formed the surface climate daily value dataset (V3.0) of the China Meteorological Data Network (http://data.cma.cn/). The data were quality controlled. We focused on the extended summer period covering the months May–September to account for the impacts of early and late summer heatwaves (Y. Chen et al., 2021). Four sets of random validation stations were selected to make their distribution more uniform. Containing of 10% of all stations, a total of 69, each set randomly selects one day of the month to apply, so a total of

four days per month using only interpolation points for interpolation. Some random validation stations overlap, so we obtained a validation set of 241 points and a training set of 450 points.

Data on elevation and geographical and administrative divisions were obtained from the Resource and Environmental Science and Data Center of the Chinese Academy of Sciences (https://www.resdc.cn/). The geographical divisions used in this study were as follows: North (N) consisted of Beijing, Tianjin, Hebei, Shanxi, and Inner Mongolia; Northwest (NW) consisted of Xinjiang, Qinghai, Gansu, Ningxia, and Shaanxi; Northeast (NE) consisted of Heilongjiang, Jilin, and Liaoning; Southwest (SW) consisted of Tibet, Yunnan, Sichuan, Chongqing, and Guizhou; Southcentral (SC) consisted of Henan, Hubei, Hunan, Guangdong, and Guangxi; and East (E) consisted of Shandong, Anhui, Jiangsu, Shanghai, Zhejiang, Jiangxi, and Fujian (Figure 1). The data on administrative divisions involved 34 provincial administrative units, 371 municipal units, and 2902 county units.

In this study, the municipalities directly under the central government were compared with cities at the prefecture level, with the latter classified as cities. To investigate the heatwave hazards in cities at different levels of economic development, we used the city ranking data from the Rising LAB (The Rising LAB, 2021). Based on commercial resource concentration, city hubs, city people's activity, lifestyle diversity, and future plasticity, the Rising LAB constructed an index model of cities' business attractiveness and divided 337 cities into six categories: four first-tier cities, 15 new first-tier cities, 30 second-tier cities, 70 third-tier cities, 90 fourth-tier cities, and 128 fifth-tier cities.

2.3 Data preparation

2.3.1 Meteorological data spatial interpolation

At present, the methods for obtaining meteorological data of a region by spatial interpolation of discrete meteorological stations mainly include inverse distance weighting (IDW) (Tanır Kayıkçı & Zengin Kazancı, 2016), Kriging (Yin et al., 2020), parameter-elevation regressions on independent slopes model (PRISM), the trend surface analysis (TSA), and thin plate smoothing spline (TPS) (Qian et al., 2010). Among them, Kriging and IDW are the most widely used in practical applications; however, their interpolation accuracies are not high enough for unevenly distributed meteorological data and complex terrains (Shu et al., 2011). TPS based

on the principle of minimum curvature uses the characteristics of smoothly distributed meteorological elements in space to fit the surface, which is more reflective of the natural spatial distribution of things (Hutchinson & Gessler, 1994). The Australian National University Spline (ANUSPLIN) is a special meteorological data space interpolation program based on TPS that can effectively simulate terrain. It has been proven to be a reliable software for meteorological data interpolation (Feng et al., 2021; Price et al., 2000), and its interpolation accuracy in complex terrain areas is better than that of other methods (Jia & Cui, 2018; Yi et al., 2020). It can complete the spatial interpolation of more than two surfaces at the same time, so it is especially suitable for the interpolation of time series meteorological data (Hutchinson & Xu, 2013; M. Zhao et al., 2021).

Thus, in this study, we used the ANUSPLIN to interpolate MT and RH with the help of a one-dimensional independent covariate (the elevation data)

2.3.2 Interpolation accuracy validation

The accurate interpolation of MT and RH forms the premise for calculating heatwave properties. Therefore, the cross-validation method was used to verify the MT and RH datasets, and the process was as follows:

- The mean absolute error (MAE), normalized mean absolute error (NMAE), root mean square error (RMSE), and normalized root mean square error (NRMSE) values were calculated for the units of different timescales (day, month, year) using the validation set results as the true values and the interpolated results as the predicted values.
- The predicted values were fitted as independent variables and the true values as dependent variables, and the slope, R2, and P values were calculated for the different timescale units.
- A total of 18 cross-validation results for the two variables—that is, MT and RH—were selected according to the descending order of R2 at the different timescales for presentation; the numbers selected were for Day 4, Month 3, and Year 2.

The results in Table 1 showed that the minimum MAE values for the MT and RH interpolations were 0.80℃ and 3.45%, respectively. The minimum RMSEs were 1.03℃ and 4.76%, respectively. The minimum R2 value was 0.5318, but 98.08% of the results were not

lower than 0.7, indicating that the prediction values were highly correlated with the true values ($P < 0.001$). The verification results showed that the interpolation results based on ANUSPLIN were accurate and reliable. Therefore, the MT and RH datasets could be used to calculate TI and HI.

Table 1 also presents the 18 cross-validation results obtained for the two variables, where $0.98 < slope < 1.0$, $R2 > 0.9$, and the results passed the significance test ($P < 0.01$), as well as the NMAE and NRMSE calculated using the max–min normalization method.

Table 1. Interpolation verification results

Date	Variable	slope	R^2	P	MAE	NMAE	RMSE	NRMSE
May 22, 1994	RH	0.9883	0.9585	$1.2 \times e^{-47}$	3.6425	0	4.8385	0
May 5, 2002	RH	0.9906	0.9393	$8.9 \times e^{-43}$	4.4610	0.6736	5.6748	0.4558
May 22,2010	RH	0.9853	0.9390	$1 \times e^{-42}$	4.4661	0.6777	5.8611	0.5574
May 22,2016	RH	0.9855	0.9427	$5.25 \times e^{-43}$	3.9316	0.2379	5.3401	0.2734
May 1997	RH	0.9940	0.9078	$4.58 \times e^{-142}$	4.8122	0.9625	6.3506	0.8241
May 1999	RH	1.0043	0.9064	$3.53 \times e^{-141}$	4.6614	0.8384	6.4561	0.8816
May 2016	RH	0.9981	0.9156	$8.96 \times e^{-148}$	4.6932	0.8646	6.5814	0.9499
1997	RH	0.9933	0.8652	0	4.8577	1	6.6733	1
1990	RH	0.9945	0.8645	0	4.6707	0.8461	6.4122	0.8577
August 17, 1990	MT	1.0033	0.9717	$4.19 \times e^{-53}$	0.8313	0	1.0669	0
May 10, 1995	MT	1.0051	0.9654	$2.98 \times e^{-50}$	0.9118	0.2746	1.3134	0.4205
July 31, 2012	MT	1.0081	0.9664	$2.17 \times e^{-51}$	0.9017	0.2399	1.1743	0.1831
September 27, 2014	MT	0.9985	0.9659	$3.55 \times e^{-51}$	1.0061	0.5960	1.3341	0.4559
September 1992	MT	0.9996	0.9532	$6.97 \times e^{-182}$	1.0220	0.6503	1.4879	0.7182
September 2003	MT	1.0012	0.9544	$4.55 \times e^{-184}$	1.0433	0.7229	1.5320	0.7934
September 2019	MT	1.0023	0.9486	$1.24 \times e^{-177}$	0.9876	0.5330	1.4638	0.6772
1990	MT	0.9988	0.9409	0	1.1018	0.9227	1.6530	1
2003	MT	0.9994	0.9433	0	1.1245	1	1.6410	0.9796

4 Results

4.1 Dynamic changes in TI in different months

Figure 3 shows the ATI values for the five months considered over the 30-year period. In terms of TI, the high-value areas (HAs) in China were mostly located in the northwest, east, and

south, and the low-value areas (LAs) were located in the SW and NE. With the northward movement of the direct sunlight region and the influence of topography, the HAs expanded in East Xinjiang, Southeast Tibet, and Hainan in May (Figure 3a). After various regions reached high levels with different coverages in June, July, and August (Figure 3b, c, d), the HAs began to move southward in September (Figure 3e). By this time, apart from the HAs in East Xinjiang, Southeast Tibet, Guangdong, South Guangxi, and Hainan, the TI values of other areas greatly decreased. The TI of southern China was low because of the rainy season in May and June, so HAs appeared in the north (Figure 3a, b). In July and August, South China began heating up on a large scale. Affected by high relative humidity and low wind speed, the southeastern provinces of China, Sichuan, and Chongqing reached maximum TI levels and coverage in August (Figure 3c, d).

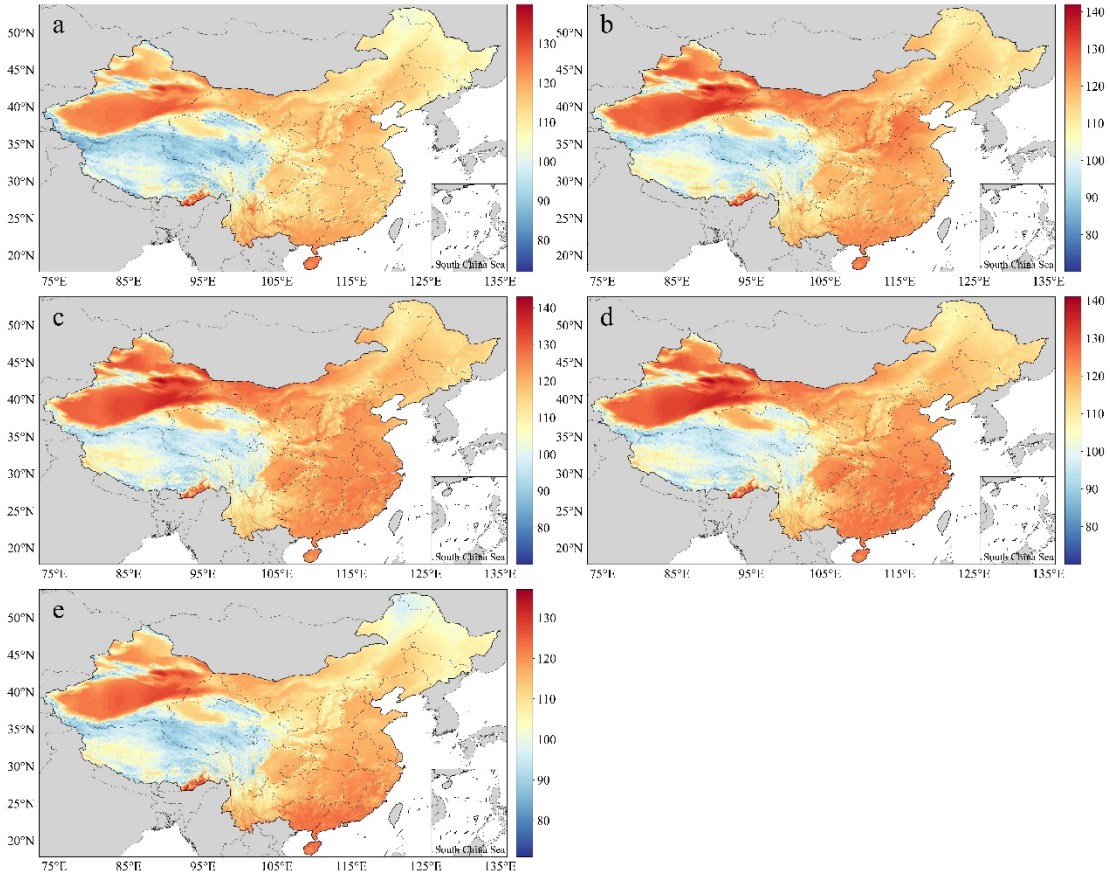

Figure 3. Spatial distribution of annual average TI (ATI) for the years 1990–2019: (**a**) May, (**b**) June, (**c**) July, (**d**) August, (**e**) September

With the time series as the independent variable and the ATI of each month over 30 years as the dependent variable, a linear regression was carried out, and the change slope was calculated. A significance test was performed. Figure 4 shows the ATI slope for the different months and the monthly slope ($P < 0.05$). A slope higher than 0 indicates that TI had a linear increasing trend, while a slope lower than 0 indicates that TI had a linearly decreasing trend. The proportions (slope > 0) were 99.99%, 99.43%, 100%, 99.03%, 98.00%, and 99.92% in the grids passing the significance test, indicating that the trend of increasing TI was widespread and significant. In May, HAs were located in Beijing, Tianjin, Shandong, Yunnan, Sichuan, etc. (Figure 4a). In June, July, and August, HAs appeared in the central and western provinces of China, East Tibet, West Yunnan, and Inner Mongolia (Figure 4b, c, d), with a continuous distribution. HAs appeared in the southeastern provinces of China in August and September as well as in Liaoning, East Inner Mongolia, and Central and West Tibet in September (Figure 4d, e), with relatively discrete distributions. The ATI dramatically increased in the regions where the slope was greater than 0.1. The monthly slope was reduced by the effect of inter-year changes, but the increasing areas passing the significance test were still consistent with the above results.

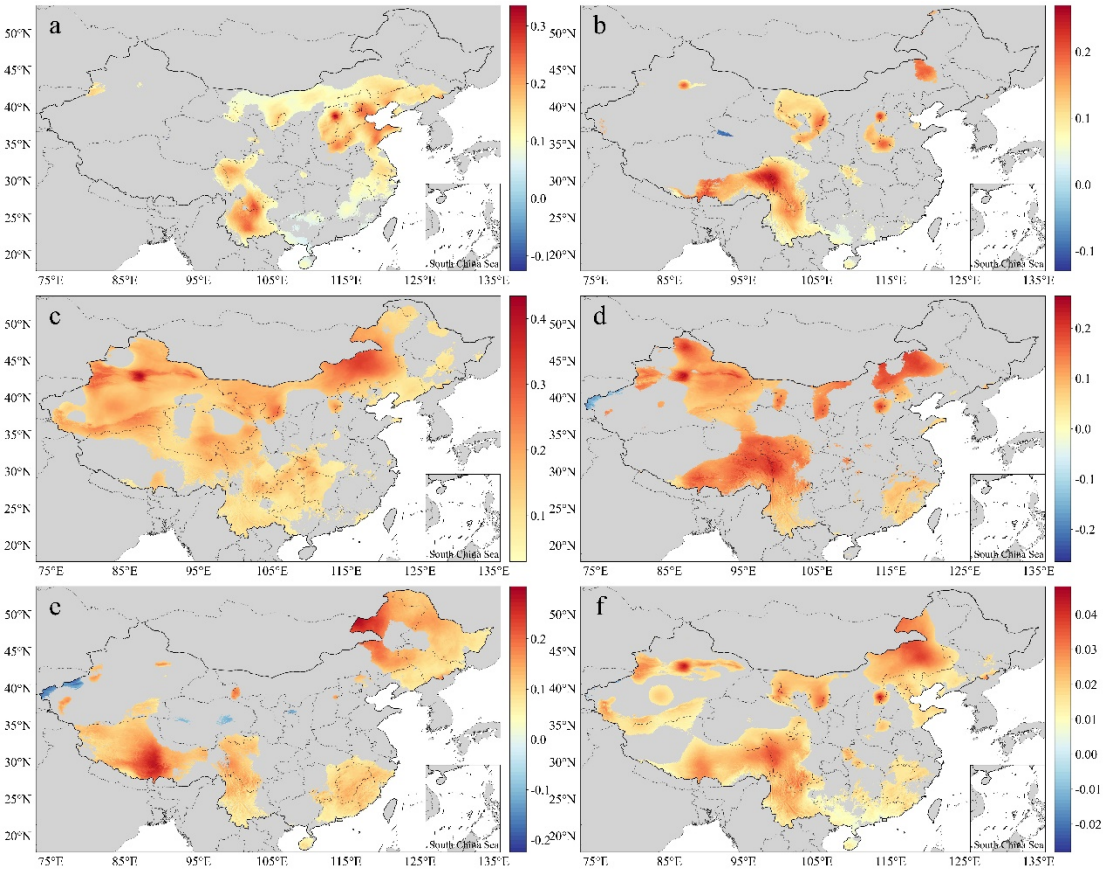

352 **Figure 4.** Slope of the mean TI: (**a**) May, (**b**) June, (**c**) July, (**d**) August, (**e**) September, (**f**)
353 monthly
354

355 Figure 5 shows the annual changes in the national ATI and the RC of the ATI for
356 different regions and different months. From 1990 to 2019, ATI was found to increase, but with
357 fluctuations. The minimum ATI value hovered around 110.5 in 1992–1994, and the maximum
358 value appeared in 2007 at about 113.5. The total ATI increase was about 1.99 over 30 years
359 (Figure 5a). The RC of ATI was the largest (3.39%) in July, and from a regional perspective, the
360 RC of ATI in descending order was N > Nation > NW > NE > SW > SC > E. The RC of ATI in
361 the SW and NE—which are regions sensitive to climate change—was higher than the national
362 average in June and September (Figure 5b).

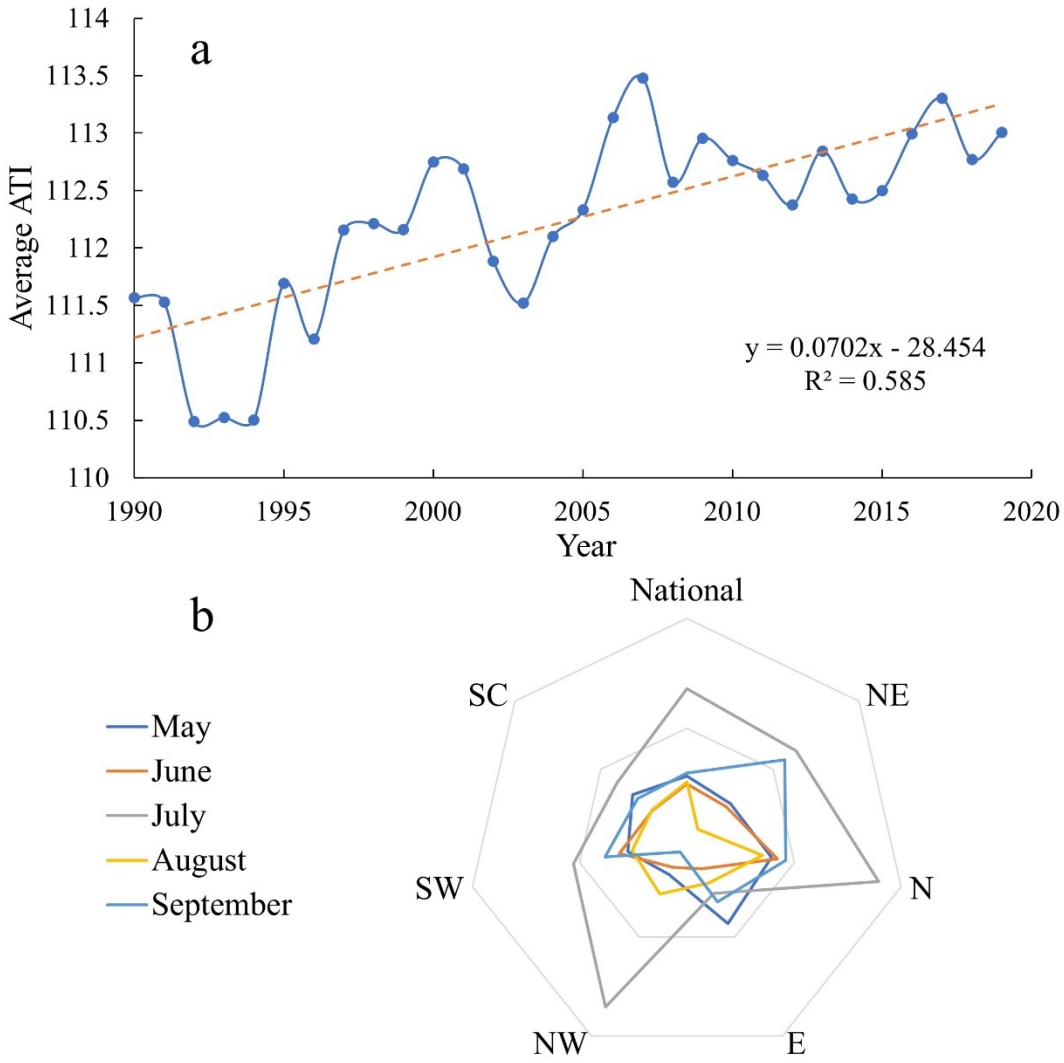

Figure 5. Annual change in the national ATI in 1990–2019 (**a**) and RC of ATI between 1990–1994 and 2015–2019 (**b**)

4.2 Assessment of hazard indicators

Figure 6 shows the annual averages and slopes of three hazard indicators, namely HWF, HWMHI, and HWMD for the years 1990–2019 ($P < 0.05$). HAs for these indicators were mostly found in the NW, E, and SC, followed by the N, and LAs were found in the NE and SW. Extremely high values were found in the southeastern region of SW (Figure 6a, c, e), and a small number of extremely high values of HWF were found in Southeast Tibet and East Xinjiang. Except for the extremely low values, the HWF for a large area of the country reached an average of 3–4 times per year and was widely distributed in the eastern provinces of China, Chongqing,

and Sichuan (Figure 6a). The maximum HWMHI in Southeast Tibet was 24–26, the highest value in the country; followed by Chongqing and East Xinjiang at 17–23; and South Hebei, East Henan, Central Zhejiang, South Hunan, Northwest Shandong, and South Shaanxi at 13–20 (Figure 6c). The distribution pattern of the HWMD was the same as that of the HWF; the highest HWMD (11–16 days) was found in East Xinjiang and Southeast Tibet, with an average of 4–8 days, and higher HWMD was about 8–10 days (Figure 6e). In terms of temporal trend, the percentages of slope > 0 in areas passing the significance tests for HWF, HWMHI, and HWMD were 99.84%, 99.98%, and 99.96%, respectively, indicating that heatwave frequency, intensity, and duration increased in most of the regions where significant changes occurred, such as Southwest Xinjiang, West Inner Mongolia, Chongqing, Henan, Shandong, Jiangsu, Zhejiang, and Hunan (Figure 6b, d, f).

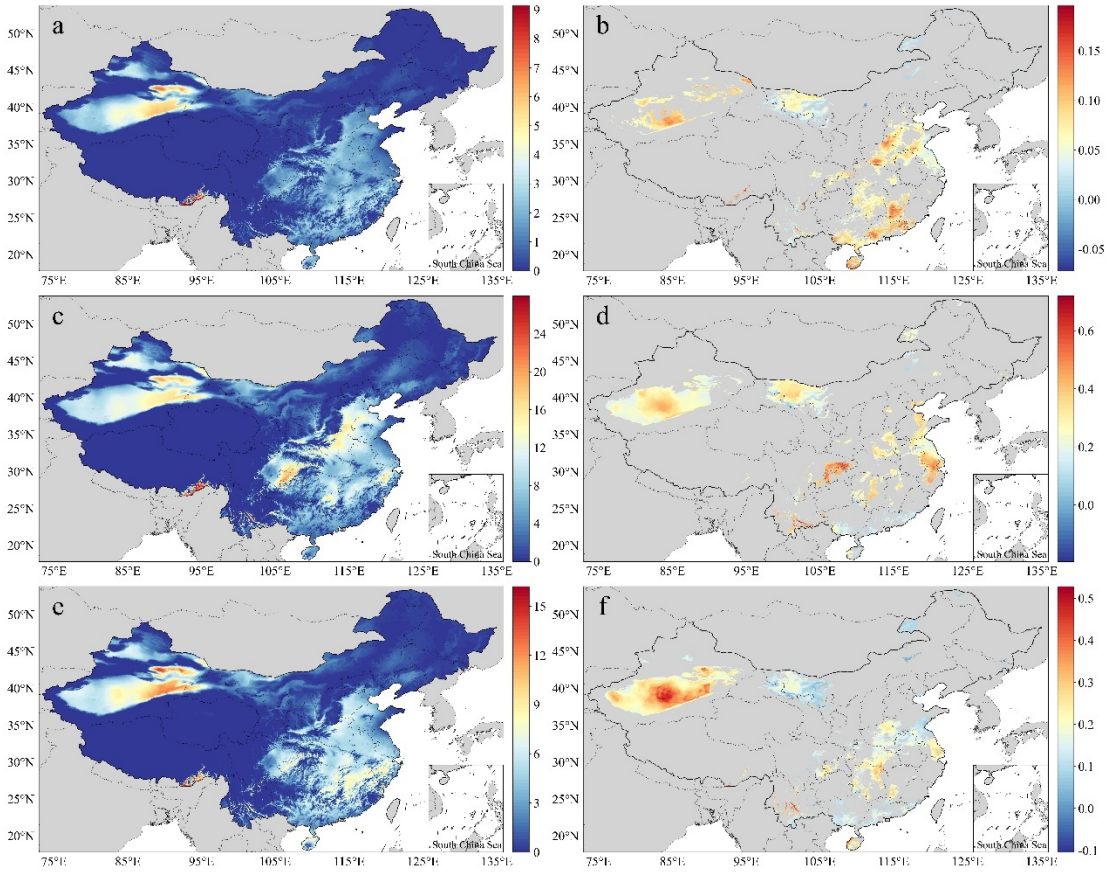

Figure 6. Spatial distribution of the averages and slopes of HWF (a, b), HWMHI (c, d), and HWMD (e, f) for the years 1990–2019

Figure 7 shows the RC levels of HWF, HWMHI, and HWMD. It can be seen that the RC of HWF descended to N > SC > NE > 0.8 > Nation > E > NW > SW, the RC of HWMHI descended to N > NE > NW > 0.8 > Nation > E > SW > SC, and the RC of HWMD descended to NW > N > SC > 0.8 > NE > E > SW > Nation. All results were greater than 0, which means that the values of all indicators increased in all regions, and each indicator sharply increased in some regions. 2–3 sharply increasing indicators were found in the N, NE, NW, and SC regions; therefore, a sharper increase occurred in northern China than in southern China. The largest RC was that of the HWMD, and it occurred in the NW. The smallest RC, too, was that of the HWMD, and it occurred in the overall nation.

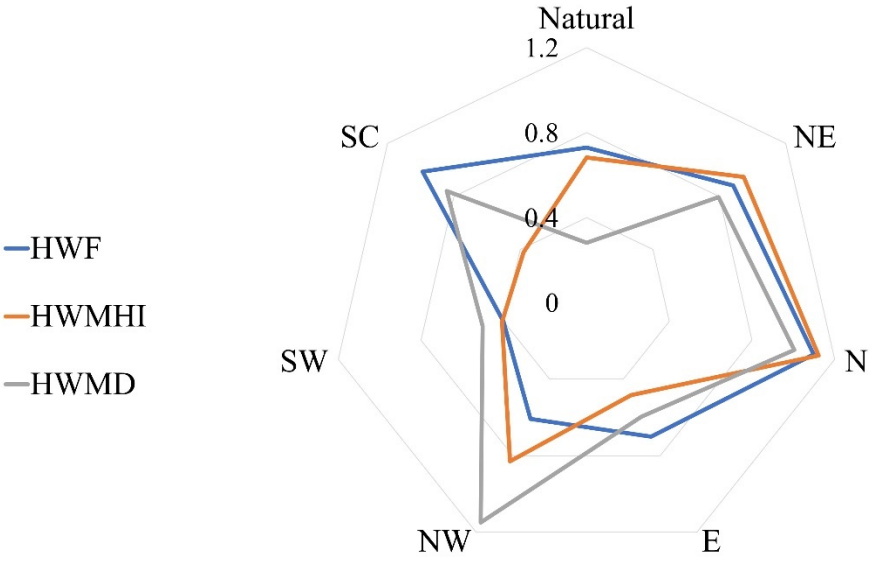

Figure 7. RC values of HWF, HWMHI, and HWMD

4.3 Spatiotemporal distribution of heatwave hazard

Figure 8a shows the AH spatial distribution in China for the years 1990–2019. The proportions of low, medium low, medium, medium high, and high AH were 61.07%, 16.77%, 13.07%, 7.06%, and 2.03%, respectively. Areas with AH levels medium and above were mainly distributed in the eastern and southern provinces of China, Southeast Tibet, East and South Xinjiang, and Chongqing. Low AH areas were mainly in the Qinghai–Tibet Plateau and the northeastern provinces of China due to their high altitudes and latitudes. Although the rates of increase in these regions were high, they could not reach the heatwave standard in the short term.

Figure 8b shows the regression results of the AH values to assess the annual changes in hazard levels. Except for a few regions, the hazard levels of regions that passed the significance test all increased in varying degrees, including the eastern provinces of China, South Xinjiang, and Western Inner Mongolia.

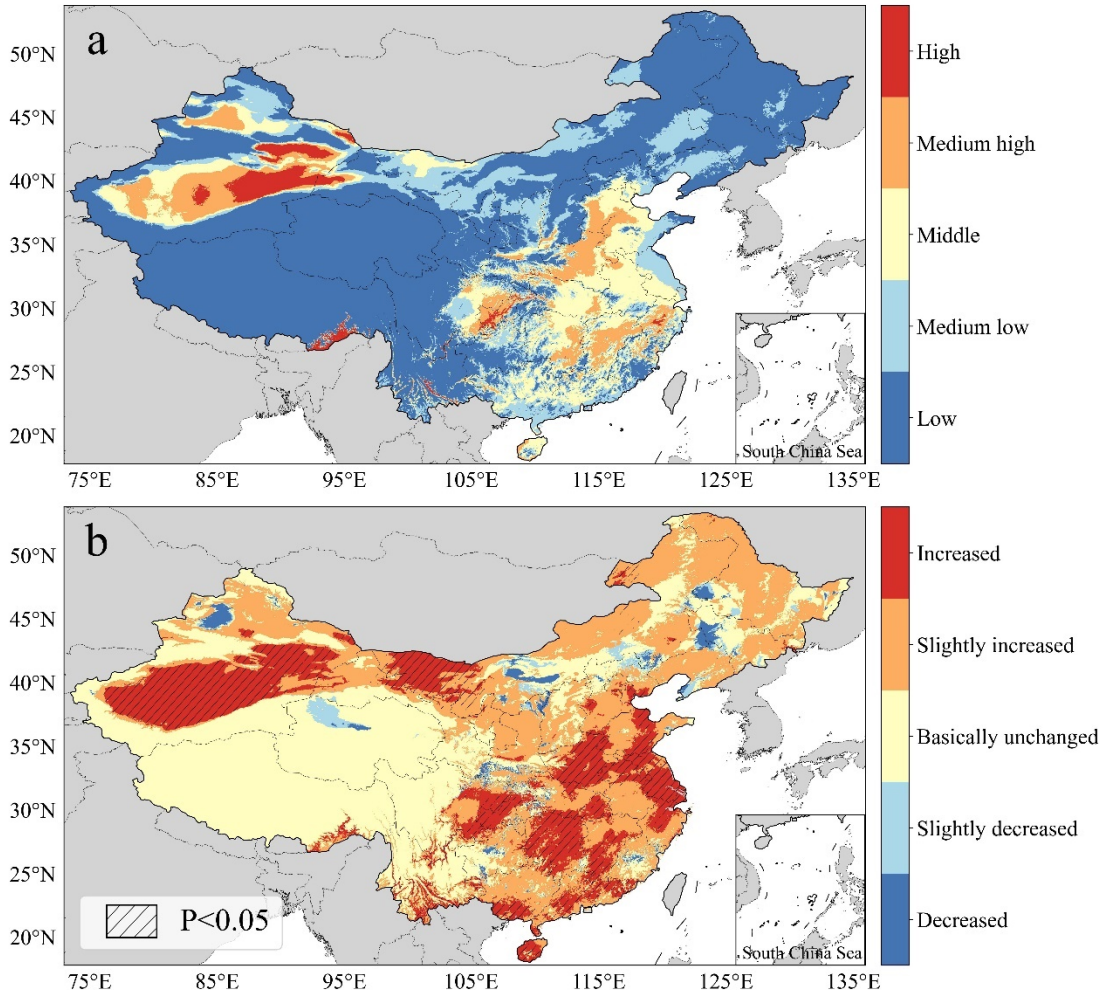

Figure 8. Heatwave hazard assessment (**a**) and slope of heatwave AH values (**b**)

The visualization results of the spatiotemporal distribution of heatwave hazards in China are shown in Figure 9. The first category of area accounted for 8.71% and included Southeast Tibet, South Xinjiang, Chongqing, South Hebei, West Henan, Central Zhejiang, Central and South Jiangxi, and East Hunan; the second category accounted for 0.38%, and the distribution area was concentrated in Northwest Xinjiang, which means that the hazard levels of almost all

high hazard areas were increasing; the third category accounted for 41.33%, with a wide distribution area in East, South, and North China, which means that most of the low hazard areas saw an increasing hazard trend that will continue to increase in the future. The spatiotemporal hazard levels of other areas, such as the Qinghai–Tibet Plateau, Yunnan–Guizhou Plateau, and parts of Northeast China, were low due to their high altitudes and latitudes.

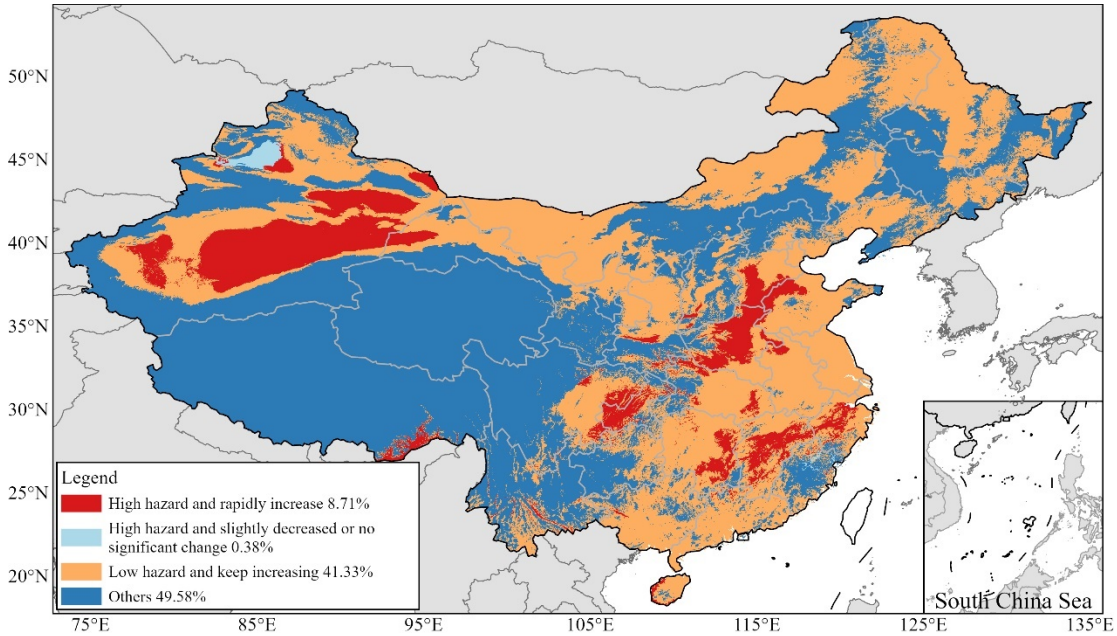

Figure 9. Heatwave classifications in China

4.4 Ranking the heatwave hazard levels of Chinese cities

We evaluated the AH values at the city and county levels and their slopes. The top 100 results at the city and county levels are shown in Table S1 and Table S2, respectively, and 10 cities and 10 counties with the fastest increase in hazard values are presented in bold; Table S1 shows the AH values of the first-tier, new first-tier, and second-tier cities. Luohe (Henan) was found to have the highest AH, while Suzhou (Jiangsu) had the highest slope (Table S1). Shanghai and the Gulou, Shunhe Huizi, Yuwangtai, Longting, Xiangfu districts in Henan Kaifeng, Wancheng District in Henan Nanyang, and Xiangcheng District in Jiangsu Suzhou were in the top ten fastest increase cities and counties but not in the top 100 AH rankings, which means the AH values of these regions were not high, but their growth rates were at the forefront. The administrative districts that passed the significance test are marked with "*" in the tables (P

438 < 0.05), and the proportion of units that significantly increased, as seen in Table S1 and Table
439 S2, were 57% and 68%, respectively, at the city and county levels.

440 Beijing, Chongqing, Tianjin, and Shanghai had relatively low rankings overall (Table 2),
441 but some urban districts in Chongqing had higher rankings at the county level (Table S2); the
442 possible reason for this phenomenon is that the presence of suburbs reduced the statistical
443 significance of mentioned cities. The top 10 first-tier, new first-tier, and second-tier cities were
444 Jinhua, Zhengzhou, Nanchang, Wuhan, Shaoxing, Changsha, Shijiazhuang, Nanjing, Wuxi, and
445 Changzhou; and the top 10 provincial capitals were Zhengzhou, Nanchang, Wuhan, Changsha,
446 Shijiazhuang, Nanjing, Hangzhou, Haikou, Chongqing, and Hefei, and these were termed the
447 "Ten Furnaces" in this study.

448 **Table 2.** AH ranking of first-tier, new first-tier and second-tier cities

index	City	index	City	index	City	index	City
1	Jinhua, Zhejiang	14	Chongqing	27	Zhongshan, Guangdong	40	City of Yantai
2	*Zhengzhou, Henan	15	Hefei, Anhui	28	*Nanning, Guangxi	41	Guiyang, Guizhou
3	Nanchang, Jiangxi	16	*Xuzhou, Jiangsu	29	*Nantong, Jiangsu	42	*Xiamen, Fujian
4	*Wuhan, Hubei	17	*Suzhou, Jiangsu	30	Taizhou, Zhejiang	43	Taiyuan, Shanxi
5	Shaoxing, Zhejiang	18	*Foshan, Guangdong	31	Beijing	44	Harbin, Heilongjiang
6	*Changsha, Hunan	19	Jinan, Shandong	32	*Huizhou, Guangdong	45	Dalian, Liaoning
7	Shijiazhuang, Hebei	20	Tianjin	33	Chengdu, Sichuan	46	Lanzhou, Gansu
8	*Nanjing, Jiangsu	21	*Yangzhou, Jiangsu	34	Fuzhou, Fujian	47	Changchun, Jilin
9	*Wuxi, Jiangsu	22	Dongguan, Guangdong	35	Wenzhou, Zhejiang	48	*Kunming, Yunnan
10	*Changzhou, Jiangsu	23	*Shanghai	36	Shenzhen, Guangdong	49	*Quanzhou, Fujian
11	*Jiaxing, Zhejiang	24	*Guangzhou, Guangdong	37	Shenyang, Liaoning		
12	Hangzhou, Zhejiang	25	Ningbo, Zhejiang	38	Zhuhai, Guangdong		
13	Haikou, Hainan	26	Xi'an, Shaanxi	39	Qingdao, Shandong		

449 Note: * means that the city passed the significance test

450 **5 Discussions**

451 5.1 Heatwave hazards in Chinese mainland

452 In 2013, severely high temperatures occurred in South China, resulting in extreme
453 drought and food production reduction (Wikipedia, 2021). In the summer of 2018, heatwaves in
454 Northeast Asia and East Asia caused more than 64.7 million mu of arable land to dry up, and
455 more than 4.6 million people faced a shortage of drinking water (China Meteorological

Administration, 2018). Figure 10 shows the heatwave indicators in 2013 and 2018. It can be seen that the present study successfully detected these heatwave events. In 2013, 4–6 heatwaves were detected in the Yangtze River Basin (1–4 in other years) (Figure 10a), HWMHI reached 18–30 (Figure 10c), the longest heatwave lasted 10–20 days, and a heatwave lasting 23 days occurred in Central and North Hunan (Figure 10e). The heatwaves in Northeast China in 2018 mainly occurred in two regions: the junction of Central South Heilongjiang and Northeast Jilin and the junction of Liaoning and Southeast Jilin. There were 2–4 heatwaves during this period (Figure 10b); HWMHI was as high as 20–25 and slightly higher than that in North China (Figure 10d), and the longest heatwave lasted 5–10 days, which was an abrupt year compared to the other years.

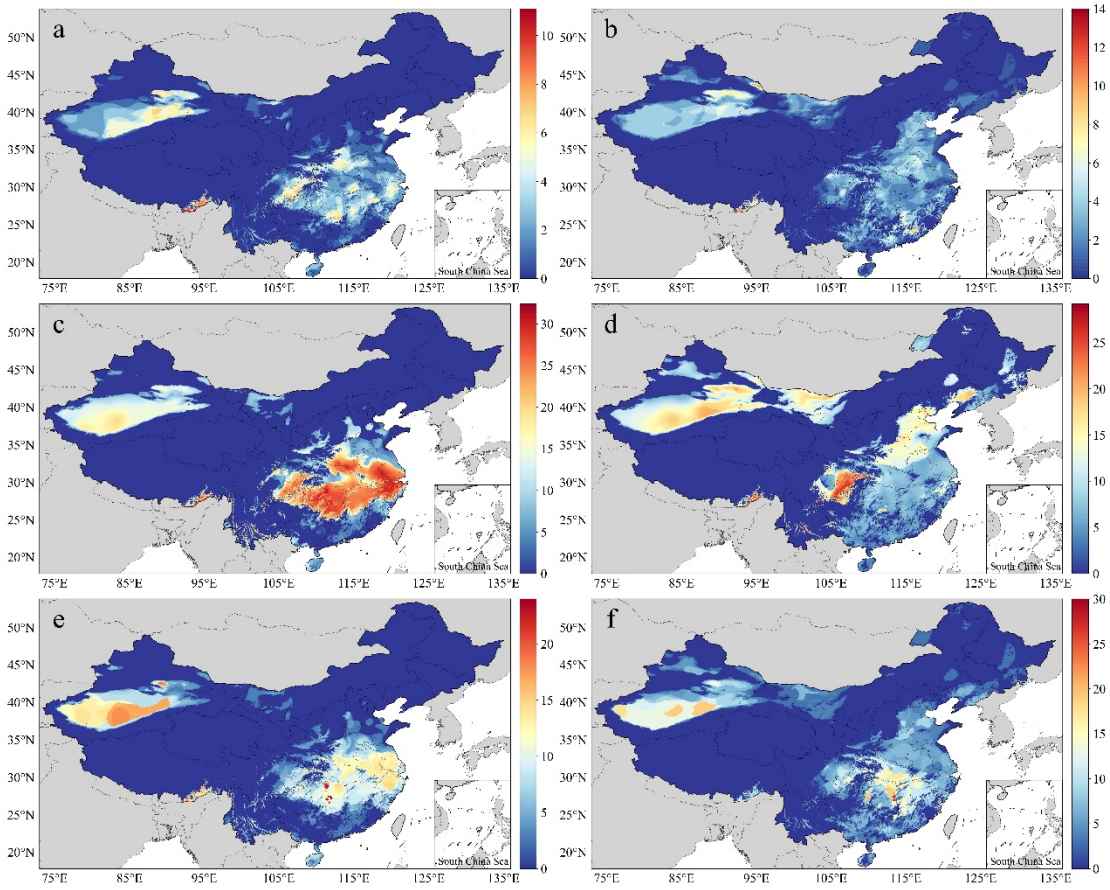

Figure 10. HWF, HWMHI, and HWMD in 2013 (**a**, **c**, **e**) and 2018 (**b**, **d**, **f**)

The present study showed an obvious upward trend in the Northeast and the Qinghai–Tibet Plateau during TI, which aligns with the results of previous studies (Bibi et al., 2018; Fan

et al., 2011; Q. Wang et al., 2020; J. Zhang et al., 2019). We further verified the reliability of the results by comparing them with those of past research. Figure 11 shows a map of the heatwave hazards in the Belt and Road area based on relative and absolute thresholds from Yin's study(Yin et al., 2020), indicating that East China and North and Southeast Asia are high-hazard areas. Comparing this with the present research (Figure 9) revealed good consistency in the results of the eastern, northeastern, and northwestern regions of China; high-hazard areas, such as Southeast Tibet, East Xinjiang, Chongqing, and other regions, were accurately identified. However, the results obtained for South China, such as the Hainan and Guangxi regions, were quite different, mainly because the definition in past research only included the annual relative temperature threshold and not the long-term changes. Thus, Yin's results overestimate the hazard. In addition, Yin's study involved more tropical and arctic regions, thus reducing the differences seen within China. To make the results comparable between years, it is also necessary to normalize the annual indicators using a unified threshold, and it is unreasonable to simply normalize them to 0–1, which is another issue in his study. In contrast, the results of the heatwave hazard assessment in this study are more consistent with those of existing studies; they are also more accurate and better reflect the hazard levels in China.

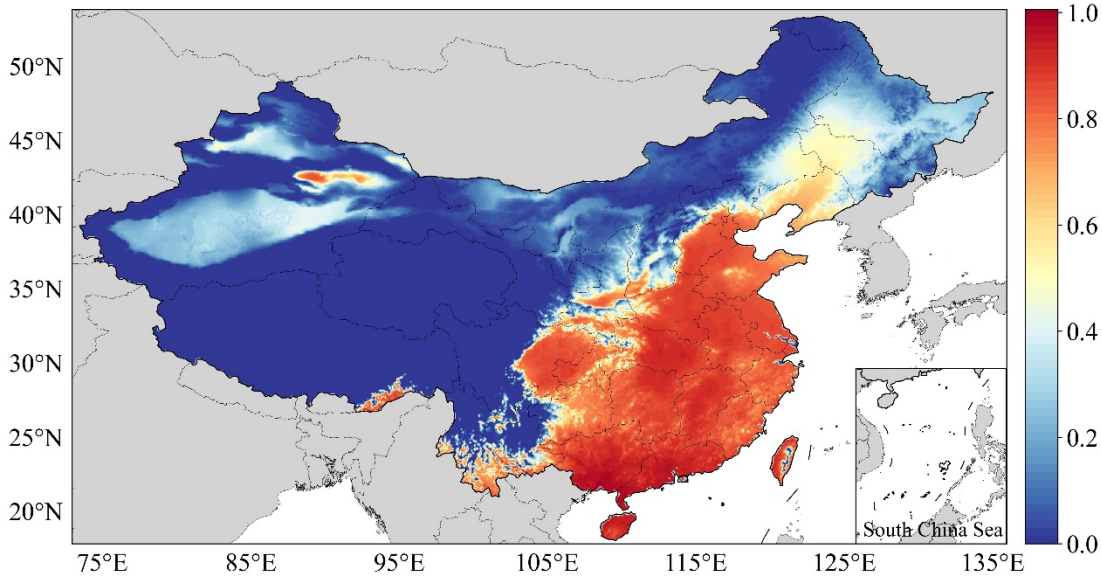

Figure 11. Heatwave hazard assessment (Yin et al.)

Several studies have shown that urban heat islands and heat waves synergistically increase the overall risk levels of cities (He, Wang, et al., 2022; Zong et al., 2021). In 2017, the

China Meteorological Administration released the rankings of hot summer cities in China, which included Chongqing, Fuzhou, Hangzhou, Nanchang, Changsha, Wuhan, Xi'an, Nanjing, Hefei, and Nanning; therefore, these are known as the "Ten Furnaces" (National Climate Center, 2017). A similar conclusion was drawn in the present study about the new "Ten Furnaces," as mentioned above. While the previously reported results differ slightly from ours, they are similar overall. Specifically, seven of the originally reported cities, including Nanchang and Wuhan, remained in the "Ten Furnaces" identified in the present study, while Nanning, Xi'an, and Fuzhou were replaced by Zhengzhou, Shijiazhuang, and Haikou. This was due to the differences in the research scale (point scale and grid scale) and the calculated standards (HI and heatwave hazard). Zhengzhou, Wuhan, Changsha, and Nanjing were found to have a significant increase in hazard levels. Previous research has pointed out that the North China Plain is threatened by deadly heatwaves (Kang & Eltahir, 2018), which provides another explanation for the cities in North China becoming "Furnace Cities." Notably, Jinhua (Zhejiang) ranked first in terms of AH, and this result is similar to that of past research (S. Wang, 2021). The possible reason for this is that Jinhua is surrounded by mountains and experiences rapid warming during the day and slow cooling at night (X. Liu & Huang, 2015). Research shows that defining city classes, which was the method used in this study, can help focus on cities that are easily overlooked in heatwave research.

5.2 Strengths and limitations of the study

Previous studies have pointed out that extreme regional heatwaves will increase significantly with global warming (Dosio et al., 2018; Guo et al., 2017; Y. Zhang et al., 2019), while temporal or spatial compounding heatwave events will further increase heat-related hazards (An & Zuo, 2021; Baldwin et al., 2019; Y. Chen et al., 2021). The traditional hazard assessment of heatwaves only considers temperature variables, which may lead to inaccuracies in dry and wet areas. Compared to studies that only consider temperatures, the present study can better reflect people's feelings. In addition, the hazard assessment of China's heatwaves at the grid scale, particularly with a spatial resolution of 0.01°, was more refined than those of meteorological stations and can help intuitively describe the heatwave grades in different regions. Third, while heat wave research tends to focus more on cities due to the impact of urban heat islands (He, Wang, et al., 2022; Savić et al., 2018; Zong et al., 2021), there exist a large

number of farmers and migrant workers in the vast Chinese mainland who are relatively poor and need to work outdoors, with their jobs being poorly mechanized due to topography; this means that they will be exposed to hot weather for long periods of time. There is spatial continuity in the present study's results, as they focus on county village areas, and may be used to provide assistance to the inhabitants of these areas from a heatwave perspective and in the context of China's policy of precise poverty alleviation.

However, it should be noted that the relationship between heatwaves and human health is extremely complex, so the somatosensory temperatures used in different studies are not unique. In some cases, the adverse effects on humans may have been overestimated (such as the narrow tube effect between large high-rise buildings) or underestimated (such as strong solar radiation outdoors) (Sylla et al., 2018), but the effects of radiation and wind speed on the human body are relatively insignificant. Therefore, the indicators selected for this study did not consider the effects of wind speed and the underlying surface. The effects of somatosensory temperature were relatively insignificant (F. Wang et al., 2021). In addition, this study did not distinguish the different indicators based on their importance for calculating heatwave hazards; this is also a limitation of the study because different regions and different indicators have different effects on hazards.

5.3 Implications for future heatwave research and public policy

Previous studies have shown that the additional mortality caused by the first heatwave is 5.04%, which is higher than that after (2.65%), and that the length of the heatwave season is increasing (Habeeb et al., 2015). Heatwaves affect the thermoregulatory system of organisms through heat stress, thus causing harm to organisms and the natural world (Xu & Tong, 2017). Past studies have also shown that the faster the temperature changes, the higher the heat stress and the greater the harm to human blood vessels (Calleja-Agius et al., 2021; C. Liu et al., 2015). Therefore, it is necessary to pay extra attention to heatwave characteristics such as heatwave start and end dates and different heatwave grades. These characteristics can also provide us with a heatwave's spatial and temporal information. In fact, the grid datasets for TI and HI in China were convenient for heatwave characteristics research.

Several areas highlighted in Figure 6 need our attention, including Southeast Tibet, East Xinjiang, Chongqing, North Henan, and Central Zhejiang. The values of the heatwave indicators

in Chongqing and Central Zhejiang were much higher than the national average, and the population is growing due to economic construction and tourism, raising the need to pay more attention to these regions. The government should rationally determine the schedules of outdoor workers (such as sanitation workers, construction workers, etc.) based on the heatwave characteristics of different regions, and other social organizations should actively publicize relevant heatwave prevention knowledge to reduce the possibility of residents being exposed to high temperatures and humidity levels for extended durations, thus reducing the possibility of heatwaves harming their health. The medium and high hazard areas were divided into two parts (Li X. et al., 2021; Z. Li et al., 2019), of which the eastern part has a developed economy and high population density; heatwaves will thus continue to have a deep impact on human society. This part should receive special attention when formulating policies, especially Chongqing, North Henan, Central Zhejiang, Central and South Hunan, and Central and South Jiangxi. Although the hazard level of the western part is higher, heatwaves have less impact on society due to the underdeveloped economy and relatively low population. In addition, several areas with low spatiotemporal hazard levels were identified in this study; the ecological protection and construction of these areas should not be neglected, especially considering their high sensitivities to climate change and high ecological vulnerability.

It is now possible to accurately forecast heatwave weather, and potential deaths due to heatwaves can be avoided via the joint efforts of the government, individuals, and caregivers of at-risk people (Cheng et al., 2018). Previous studies have shown that the success of a heatwave warning system can result in a large amount of people being saved as well as in high profits (Cheng et al., 2018; C. Huang et al., 2013). However, social heatwave handling systems need to be further researched in the context of carbon neutrality policies. The demand for electric power will be difficult to meet under the combined pressure of soaring electricity use and drought, which is more prevalent in the southern regions of China during heatwaves, as these areas rely more on hydropower. The present study's results also pointed out some of these regions.

In addition, meteorological disasters, such as hot, dry winds and forest fires caused by heatwaves, will also have impacts on agriculture and forestry, leading to the loss of human society. In severe cases, these will threaten human health and even life safety. If a more comprehensive assessment of heatwaves hazards is required in the future, the indicators that directly or indirectly pose health threats to humans should be focused on.

6 Conclusion

Based on the interpolated MT and RH data, we calculated the values for TI and HWI. Based on HWI, the datasets of HWF, HWMHI, and HWMD in the Chinese mainland, covering the years 1990–2019, were obtained with a spatial resolution of 0.01°, and their spatiotemporal distribution was analyzed. Then, the spatiotemporal distribution of heatwave hazards was evaluated. The results revealed the following:

(1) TI increased in 1990–2019, albeit with fluctuations, with the highest ATIRC found in North China, followed by Northwest China, in July (3.39%). Notably, there was a clear trend of increasing TI in climate-sensitive regions, such as Northeast China and the Qinghai–Tibet Plateau, in June and September.

(2) Areas with hazard levels of medium and above were mainly distributed in East and South China, Southeast Tibet, East and South Xinjiang, and Chongqing, accounting for 22.16%; areas with significantly increasing hazard levels were East China, South Xinjiang, and Western Inner Mongolia. Through comparative analysis, areas with "high and rapidly increasing" hazard levels, such as Southeast Tibet, South Xinjiang, Chongqing, South Hebei, West Henan, Central Zhejiang, Central and South Jiangxi, and East Hunan, accounted for 8.71% of the country, and areas with "low and keep increasing" hazard levels were widely distributed in the eastern, southern, and northern regions of China, including Jiangsu, Inner Mongolia, Hainan, Shandong, and Heilongjiang, and accounted for 41.33%.

(3) The city with the highest AH was Luohe (Henan), and the city with the fastest growth was Suzhou (Jiangsu). The units of cities and counties were found to have increased significantly by 57% and 68%, respectively. Among the 49 first-tier, new first-tier, and second-tier cities, the top 10 were Jinhua, Zhengzhou, Nanchang, Wuhan, Shaoxing, Changsha, Shijiazhuang, Nanjing, Wuxi, and Changzhou. Some of these cities have low administrative or economic development levels, which have reduced people's attention to the mentioned cities. However, it is necessary to pay attention to the internal infrastructure construction in these cities to reduce the harm of future heatwaves. Upon ranking the provincial capitals, the "Ten Furnaces" were identified as Zhengzhou, Nanchang, Wuhan, Changsha, Shijiazhuang, Nanjing, Hangzhou, Haikou, Chongqing, and Hefei (sequentially).

Acknowledgments

Author Contributions Statement: Qingsheng Liu: Conceptualization, Writing - Review & Editing, Supervision, Project administration, Funding Acquisition; Wei Wu: Methodology, Software, Validation, Formal analysis, Resources, Data Curation, Writing - Original Draft, Visualization; He Li: Writing - Review & Editing, Resources; Chong Huang: Conceptualization, Writing - Review & Editing.

Thanks are due to Xintong Zheng for assistance with the experiments and to Xin Dai and Xilin Wu for valuable discussion. This study was funded by the Strategic Priority Research Program of the Chinese Academy of Sciences (Project No. XDA20030302), and the Innovation Project of LREIS (Project Nos. 088RA20CYA)

Open research (availability statement)

Maximum temperature (MT,°C) and average relative humidity (RH, %) data from 699 meteorological stations in China for the years 1990–2019 were used to calculate the TI and HI; these formed the surface climate daily value dataset (V3.0) of the China Meteorological Data Network (http://data.cma.cn/). Due to the large amount of data, The gridded dataset (0.01°) interpolated and processed by authors includes daily TI and HI, temporal and spatial characteristics of annual heatwave indicators and heatwave hazard will be shared in an appropriate manner. Figures were created mainly by Python, Arcgis Pro and Excel, the script files related to this manuscript have been uploaded to Github, https://github.com/wuming365/china-contourf

References

Alduchov, O. A., & Eskridge, R. E. (1996). Improved Magnus Form Approximation of Saturation Vapor Pressure. Journal of Applied Meteorology and Climatology, 35(4), 601–609. https://doi.org/10.1175/1520-0450(1996)035<0601:IMFAOS>2.0.CO;2

An, N., & Zuo, Z. (2021). Changing structures of summertime heatwaves over China during 1961–2017. Science China Earth Sciences, 64(08), 1242–1253.

Anderson, G. B., & Bell, M. L. (2011). Heat Waves in the United States: Mortality Risk during Heat Waves and Effect Modification by Heat Wave Characteristics in 43 U.S. Communities. Environ Health Perspect, 119(2), 210–218. https://doi.org/10.1289/ehp.1002313

Armstrong, B., Sera, F., Vicedo, -Cabrera Ana Maria, Abrutzky, R., Åstr, öm D. O., Bell, M. L., Chen, B.-Y., de, S. Z. S. C. M., Correa, P. M., Dang, T. N., Diaz, M. H., Dung, D. V., Forsberg, B., Goodman, P., Guo, Y.-L. L., Guo, Y., Hashizume, M., Honda, Y., Indermitte, E., … Gasparrini, A. (2019). The Role of Humidity in Associations of High Temperature with Mortality: A Multicountry, Multicity Study. Environmental Health Perspectives, 127(9), 097007. https://doi.org/10.1289/EHP5430

Baldwin, J. W., Dessy, J. B., Vecchi, G. A., & Oppenheimer, M. (2019). Temporally Compound Heat Wave Events and Global Warming: An Emerging Hazard. Earth's Future, 7(4), 411–427. https://doi.org/10.1029/2018EF000989

Beijing Climate Center, C. M. M. A. (2021). China's Blue Book on Climate Change (2021).

Bibi, S., Wang, L., Li, X., Zhou, J., Chen, D., & Yao, T. (2018). Climatic and associated cryospheric, biospheric, and hydrological changes on the Tibetan Plateau: A review. International Journal of Climatology, 38(S1), e1–e17. https://doi.org/10.1002/joc.5411

Bobb, J. F., Peng, R. D., Bell, M. L., & Dominici, F. (2014). Heat-Related Mortality and Adaptation to Heat in the United States. Environ Health Perspect, 122(8), 811–816. https://doi.org/10.1289/ehp.1307392

Borden, K. A., & Cutter, S. L. (2008). Spatial patterns of natural hazards mortality in the United States. International Journal of Health Geographics, 7(1), 64. https://doi.org/10.1186/1476-072X-7-64

Calleja-Agius, J., England, K., & Calleja, N. (2021). The effect of global warming on mortality. Early Human Development, 155, 105222. https://doi.org/10.1016/j.earlhumdev.2020.105222

Chatterjee, P. (2019). No cause identified for death of children in Bihar, India. The Lancet, 393(10191), 2578. https://doi.org/10.1016/S0140-6736(19)31509-0

Chen, K., Huang, L., Zhou, L., Ma, Z., Bi, J., & Li, T. (2015). Spatial analysis of the effect of the 2010 heat wave on stroke mortality in Nanjing, China. Scientific Reports, 5(1), 10816. https://doi.org/10.1038/srep10816

Chen, Y., Liao, Z., Shi, Y., Tian, Y., & Zhai, P. (2021). Detectable Increases in Sequential Flood-Heatwave Events Across China During 1961–2018. Geophysical Research Letters, 48(6), e2021GL092549. https://doi.org/10.1029/2021GL092549

Cheng, J., Xu, Z., Bambrick, H., Su, H., Tong, S., & Hu, W. (2018). Heatwave and elderly mortality: An evaluation of death burden and health costs considering short-term mortality displacement. Environment International, 115, 334–342. https://doi.org/10.1016/j.envint.2018.03.041

China Meteorological Administration. (2013). Foreign high temperature standards. http://www.cma.gov.cn/2011xzt/20120816/2012060201/201208160101/201305/t20130531_215191.html

China Meteorological Administration. (2018). Interpretation: Who is "smoldering" the earth when heatwaves are raging? http://www.cma.gov.cn/2011xwzx/spxw/201808/t20180804_475250.html

Dai, X., Liu, Q., Huang, C., & Li, H. (2021). Spatiotemporal Variation Analysis of the Fine-Scale Heat Wave Risk along the Jakarta-Bandung High-Speed Railway in Indonesia. International Journal of Environmental Research and Public Health, 18(22), 12153. https://doi.org/10.3390/ijerph182212153

Dai, X., Liu, Q., Wu, X., Huang, C., & Li, H. (2021). The Risk of Heat Wave along the Jakarta-Bandung High-Speed Railway in Indonesia. Tropical Geography, 1–16.

Ding, T., Qian, W., & Yan, Z. (2010). Changes in hot days and heat waves in China during 1961–2007. International Journal of Climatology, 30(10), 1452–1462. https://doi.org/10.1002/joc.1989

Ding, Y. (2018). 2018 World Conference on the Promotion of Public Science Literacy: "Climate Change: Science and Communication Forum" [Interview]. https://chn.oversea.cnki.net/KCMS/detail/detail.aspx?dbcode=CJFD&dbname=CJFDLASN2018&filename=KJCX201810014&uniplatform=NZKPT&v=MFAq3toN%25mmd2Fl5ffyt4%25mmd2FOocHGNhbxAtHCxWfBTgeAwN%25mmd2B92jYTiNADysiEV%25mmd2BNfVUkkCD

Dong, J., Peng, J., He, X., Corcoran, J., Qiu, S., & Wang, X. (2020). Heatwave-induced human health risk assessment in megacities based on heat stress-social vulnerability-human exposure framework. Landscape and Urban Planning, 203, 103907. https://doi.org/10.1016/j.landurbplan.2020.103907

Dosio, A., Mentaschi, L., Fischer, E. M., & Wyser, K. (2018). Extreme heat waves under 1.5\hspace0.167em°C and 2\hspace0.167em°C global warming. Environmental Research Letters, 13(5), 054006. https://doi.org/10.1088/1748-9326/aab827

Emmanuel, R. (2005). Thermal comfort implications of urbanization in a warm-humid city: The Colombo Metropolitan Region (CMR), Sri Lanka. Building and Environment, 40(12), 1591–1601. https://doi.org/10.1016/j.buildenv.2004.12.004

Estoque, R. C., Ooba, M., Seposo, X. T., Togawa, T., Hijioka, Y., Takahashi, K., & Nakamura, S. (2020). Heat health risk assessment in Philippine cities using remotely sensed data and social-ecological indicators. Nature Communications, 11(1), 1581. https://doi.org/10.1038/s41467-020-15218-8

Fan, Z.-X., Bräuning, A., Thomas, A., Li, J.-B., & Cao, K.-F. (2011). Spatial and temporal temperature trends on the Yunnan Plateau (Southwest China) during 1961–2004. International Journal of Climatology, 31(14), 2078–2090. https://doi.org/10.1002/joc.2214

Feng, L., Liu, Y., Feng, Z., & Yang, S. (2021). Analysing the spatiotemporal characteristics of climate comfort in China based on 2005–2018 MODIS data. Theoretical and Applied Climatology, 143(3), 1235–1249. https://doi.org/10.1007/s00704-020-03516-6

Gu, S., Huang, C., Bai, L., Chu, C., & Liu, Q. (2016). Heat-related illness in China, summer of 2013. International Journal of Biometeorology, 60(1), 131–137. https://doi.org/10.1007/s00484-015-1011-0

Guo, X., Huang, J., Luo, Y., Zhao, Z., & Xu, Y. (2017). Projection of heat waves over China for eight different global warming targets using 12 CMIP5 models. Theoretical and Applied Climatology, 128(3), 507–522. https://doi.org/10.1007/s00704-015-1718-1

Habeeb, D., Vargo, J., & Stone, B. (2015). Rising heat wave trends in large US cities. Natural Hazards, 76(3), 1651–1665. https://doi.org/10.1007/s11069-014-1563-z

He, B.-J., Wang, J., Zhu, J., & Qi, J. (2022). Beating the urban heat: Situation, background, impacts and the way forward in China. Renewable and Sustainable Energy Reviews, 161, 112350. https://doi.org/10.1016/j.rser.2022.112350

He, B.-J., Zhao, D., Dong, X., Xiong, K., Feng, C., Qi, Q., Darko, A., Sharifi, A., & Pathak, M. (2022). Perception, physiological and psychological impacts, adaptive awareness and knowledge, and climate justice under urban heat:

A study in extremely hot-humid Chongqing, China. Sustainable Cities and Society, 79, 103685. https://doi.org/10.1016/j.scs.2022.103685

Huang, C., Barnett, A. G., Xu, Z., Chu, C., Wang, X., Turner, L. R., & Tong, S. (2013). Managing the Health Effects of Temperature in Response to Climate Change: Challenges Ahead. Environmental Health Perspectives, 121(4), 415–419. https://doi.org/10.1289/ehp.1206025

Huang, Z., Chen, H., & Tian, H. (2011). Research on the Heat Wave Index. Meteorological Monthly, 37(03), 345–351.

Hutchinson, M. F., & Gessler, P. E. (1994). Splines—More than just a smooth interpolator. Geoderma, 62(1), 45–67. https://doi.org/10.1016/0016-7061(94)90027-2

Hutchinson, & Xu, T. (2013). ANUSPLIN version 4.4 user guide. Canberra:The Australian National Universit.

Ian L. McHarg. (1969). Design With Nature. The Natural History Press.

IPCC. (2012). Managing the Risks of Extreme Events and Disasters to Advance Climate Change Adaptation: Special Report of the Intergovernmental Panel on Climate Change. Cambridge University Press. https://doi.org/10.1017/CBO9781139177245

IPCC (Ed.). (2014). Summary for Policymakers. In Climate Change 2014 – Impacts, Adaptation and Vulnerability: Part A: Global and Sectoral Aspects: Working Group II Contribution to the IPCC Fifth Assessment Report: Volume 1: Global and Sectoral Aspects (Vol. 1, pp. xv–xvi). Cambridge University Press. https://www.cambridge.org/core/books/climate-change-2014-impacts-adaptation-and-vulnerability-part-a-global-and-sectoral-aspects/summary-for-policymakers/0F96D3E32C820804D2130AE7B551D75B

IPCC. (2021). Climate Change 2021: The Physical Science Basis. Contribution of Working Group I to the Sixth Assessment Report of the Intergovernmental Panel on Climate Change [Masson-Delmotte, V., P. Zhai, A. Pirani, S.L. Connors, C. Péan, S. Berger, N. Caud, Y. Chen, L. Goldfarb, M.I. Gomis, M. Huang, K. Leitzell, E. Lonnoy, J.B.R. Matthews, T.K. Maycock, T. Waterfield, O. Yelekçi, R. Yu, and B. Zhou (eds.)]. Cambridge University Press.

Jia, Y., & Cui, P. (2018). Contrastive analysis of temperature interpolation at different time scales in the Alpine R egion by Anusplin. PLATEAU METEOROLOGY, 37(03), 757–766.

Kang, S., & Eltahir, E. A. B. (2018). North China Plain threatened by deadly heatwaves due to climate change and irrigation. Nature Communications, 9(1), 2894. https://doi.org/10.1038/s41467-018-05252-y

KNMI. (2020). heat wave standard—The Netherlands. https://www.knmi.nl/kennis-en-datacentrum/uitleg/hittegolf

Kotharkar, R., & Ghosh, A. (2021a). Review of heat wave studies and related urban policies in South Asia. Urban Climate, 36, 100777. https://doi.org/10.1016/j.uclim.2021.100777

Kotharkar, R., & Ghosh, A. (2021b). Progress in extreme heat management and warning systems: A systematic review of heat-health action plans (1995-2020). Sustainable Cities and Society, 103487. https://doi.org/10.1016/j.scs.2021.103487

Li X., Ren G., & Wang S. (2021). Change in the heatwave statistical characteristics over China during the climate warming slowdown. Atmospheric Research, 247, 105152. https://doi.org/10.1016/j.atmosres.2020.105152

749 Li, Z., Guo, X., Yang, Y., Hong, Y., Wang, Z., & You, L. (2019). Heatwave Trends and the Population Exposure
750 Over China in the 21st Century as Well as Under 1.5 °C and 2.0 °C Global Warmer Future Scenarios. Sustainability,
751 11(12), 3318. https://doi.org/10.3390/su11123318
752 Lin, H., Mo, R., & Vitart, F. (2022). The 2021 Western North American Heatwave and Its Subseasonal Predictions.
753 Geophysical Research Letters, 49(6), e2021GL097036. https://doi.org/10.1029/2021GL097036
754 Liu, C., Yavar, Z., & Sun, Q. (2015). Cardiovascular response to thermoregulatory challenges. American Journal of
755 Physiology-Heart and Circulatory Physiology, 309(11), H1793–H1812. https://doi.org/10.1152/ajpheart.00199.2015
756 Liu, X., & Huang, Y. (2015). The characteristics of climate change and atmospheric circulation characteristics of
757 high temperature days in Jinhua. Atmospheric Science Research and Application, 1, 92–99.
758 Liu, Y., & Quan, W. (2014). Research on high temperature indices of Beijing city and its spatiotemporal pattern
759 based on satellite data. Climatic and Environmental Research, 19(03), 332–342.
760 Luo, M., & Lau, N.-C. (2018). Synoptic characteristics, atmospheric controls, and long-term changes of heat waves
761 over the Indochina Peninsula. Climate Dynamics, 51(7), 2707–2723. https://doi.org/10.1007/s00382-017-4038-6
762 Masterton, J. M., Richardson, F. A., Canada, Environment Canada, Canada, & Atmospheric Environment Service.
763 (1979). Humidex: A method of quantifying human discomfort due to excessive heat and humidity. Environment
764 Canada, Atmospheric Environment. http://publications.gc.ca/collections/collection_2018/eccc/En57-23-1-79-
765 eng.pdf
766 Met Office. (2017, January 31). Heat-Health Watch. https://www.metoffice.gov.uk/public/weather/heat-
767 health/?tab=heatHealth&season=normal
768 Mitchell, D., Heaviside, C., Vardoulakis, S., Huntingford, C., Masato, G., Guillod, B. P., Frumhoff, P., Bowery, A.,
769 Wallom, D., & Allen, M. (2016). Attributing human mortality during extreme heat waves to anthropogenic climate
770 change. Environmental Research Letters, 11(7), 074006. https://doi.org/10.1088/1748-9326/11/7/074006
771 National Climate Center, C. M. A. (2017). The TOP 10 Furnace Cities in China—Hottest Cities in Summer.
772 https://www.chinahighlights.com/travelguide/article-furnace-cities.htm
773 Pengelly, L. D., Campbell, M. E., Cheng, C. S., Fu, C., Gingrich, S. E., & Macfarlane, R. (2007). Anatomy of Heat
774 Waves and Mortality in Toronto: Lessons for Public Health Protection. Canadian Journal of Public Health, 98(5),
775 364–368. https://doi.org/10.1007/BF03405420
776 Price, D. T., McKenney, D. W., Nalder, I. A., Hutchinson, M. F., & Kesteven, J. L. (2000). A comparison of two
777 statistical methods for spatial interpolation of Canadian monthly mean climate data. Agricultural and Forest
778 Meteorology, 101(2), 81–94. https://doi.org/10.1016/S0168-1923(99)00169-0
779 Qian, Y., Lv, H., & Zhang, Y. (2010). Application and assessment of spatial interpolation method on daily
780 meteorological elements based on ANUSPLIN software. JOURNAL OF METEOROLOGY AND
781 ENVIRONMENT, 26(02), 7–15.
782 Raei, E., Nikoo, M. R., AghaKouchak, A., Mazdiyasni, O., & Sadegh, M. (2018). GHWR, a multi-method global
783 heatwave and warm-spell record and toolbox. Scientific Data, 5(1), 180206. https://doi.org/10.1038/sdata.2018.206

784 Savić, S., Marković, V., Šećerov, I., Pavić, D., Arsenović, D., Milošević, D., Dolinaj, D., Nagy, I., & Pantelić, M.
785 (2018). Heat wave risk assessment and mapping in urban areas: Case study for a midsized Central European city,
786 Novi Sad (Serbia). Natural Hazards, 91(3), 891–911. https://doi.org/10.1007/s11069-017-3160-4
787 Shu, S., Liu, C., Shi, R., & Gao, W. (2011). Research on spatial interpolation of meteorological elements in Anhui
788 Province based on ANUSPLIN. Remote Sensing and Modeling of Ecosystems for Sustainability VIII, 8156, 183–
789 194. https://doi.org/10.1117/12.892263
790 Silberner, J. (2021). Heat wave causes hundreds of deaths and hospitalisations in Pacific north west. BMJ : British
791 Medical Journal (Online), 374. https://doi.org/10.1136/bmj.n1696
792 SMHI. (2020, October 9). heat wave standard—Sweden. http://www.smhi.se/kunskapsbanken/klimat/varmebolja-
793 1.22372
794 Song, X., Wang, S., Hu, Y., Yue, M., Zhang, T., Liu, Y., Tian, J., & Shang, K. (2017). Impact of ambient
795 temperature on morbidity and mortality: An overview of reviews. Science of The Total Environment, 586, 241–254.
796 https://doi.org/10.1016/j.scitotenv.2017.01.212
797 Grade of the heat wave, Pub. L. No. ICS 07.060, GB/T 29457-2012 (2012).
798 http://c.gb688.cn/bzgk/gb/showGb?type=online&hcno=DA6A2DF5B2E32753961AB5C5433DF527
799 Steadman, R. G. (1984). A Universal Scale of Apparent Temperature. Journal of Applied Meteorology, 23, 1674–
800 1687. https://doi.org/10.1175/1520-0450(1984)023<1674:AUSOAT>2.0.CO;2
801 Suarez-Gutierrez, L., Müller, W. A., Li, C., & Marotzke, J. (2020). Hotspots of extreme heat under global warming.
802 Climate Dynamics, 55(3), 429–447. https://doi.org/10.1007/s00382-020-05263-w
803 Sun, Y., Hu, T., & Zhang, X. (2018). Substantial Increase in Heat Wave Risks in China in a Future Warmer World.
804 Earth's Future, 6(11), 1528–1538. https://doi.org/10.1029/2018EF000963
805 Sylla, M. B., Faye, A., Giorgi, F., Diedhiou, A., & Kunstmann, H. (2018). Projected Heat Stress Under 1.5 °C and
806 2 °C Global Warming Scenarios Creates Unprecedented Discomfort for Humans in West Africa. Earth's Future,
807 6(7), 1029–1044. https://doi.org/10.1029/2018EF000873
808 Tanır Kayıkçı, E., & Zengin Kazancı, S. (2016). Comparison of regression-based and combined versions of Inverse
809 Distance Weighted methods for spatial interpolation of daily mean temperature data. Arabian Journal of
810 Geosciences, 9(17), 690. https://doi.org/10.1007/s12517-016-2723-0
811 The Rising LAB. (2021). Index Model of Cities' Business Attractiveness in China 2021.
812 https://www.datayicai.com/readReport/267
813 Wang, A., Tao, H., Wu, Q., Huang, J., Zhang, B., & Wang, Y. (2022). Increasing urban and rural population
814 exposures to warm-season concurrent hot days and nights on the North China Plain. International Journal of
815 Climatology. https://doi.org/10.1002/joc.7685
816 Wang, F., Zhang, J., Ge, Q., & Hao, Z. (2021). Protected changes in risk of heat waves throughout Belt and Road
817 Region in the 21st century. Chin Sci Bull, 66(23), 3045–3058. https://doi.org/10.1360/TB-2020-1171
818 Wang, Q., Zhai, P.-M., & Qin, D.-H. (2020). New perspectives on 'warming–wetting' trend in Xinjiang, China.
819 Advances in Climate Change Research, 11(3), 252–260. https://doi.org/10.1016/j.accre.2020.09.004

Wang, S. (2021). Research on spatial distribution assessment of high temperature and heat wave risk in the Yangtze River Delta region [Master, Nanjing University of Information Science & Technology]. https://doi.org/10.27248/d.cnki.gnjqc.2021.000363

Wikipedia. (2021). High temperature in China in 2013. Wikimedia Foundation. https://zh.wikipedia.org/w/index.php?title=2013%E5%B9%B4%E4%B8%AD%E5%9B%BD%E9%AB%98%E6%B8%A9&oldid=63893117

World Weather Attribution. (2021, July 7). Western North American extreme heat virtually impossible without human-caused climate change – World Weather Attribution. https://www.worldweatherattribution.org/western-north-american-extreme-heat-virtually-impossible-without-human-caused-climate-change/

Wu, X., Liu, Q., Huang, C., & Li, H. (2022). Mapping Heat-Health Vulnerability Based on Remote Sensing: A Case Study in Karachi. Remote Sensing, 14(7), 1590. https://doi.org/10.3390/rs14071590

Wu, X., Liu, Q., Liu, G., Huang, C., & Li, H. (2019). Risk assessment of heat waves: A review. Journal of Geo-Information Science, 21(07), 1029–1039.

Xu, Z., & Tong, S. (2017). Decompose the association between heatwave and mortality: Which type of heatwave is more detrimental? Environmental Research, 156, 770–774. https://doi.org/10.1016/j.envres.2017.05.005

Yaglou, C. P., & Minaed, D. (1957). Control of Heat Casualties at Military Training Centers. Arch. Indust. Health, 16(4), 302–316.

Yan, M., Xie, Y., Zhu, H., Ban, J., Gong, J., & Li, T. (2022). The exceptional heatwaves of 2017 and all-cause mortality: An assessment of nationwide health and economic impacts in China. Science of the Total Environment, 812, 152371. https://doi.org/10.1016/j.scitotenv.2021.152371

Yao, Y., & Wang, C. (2021). Variations in Summer Marine Heatwaves in the South China Sea. Journal of Geophysical Research: Oceans, 126(10), e2021JC017792. https://doi.org/10.1029/2021JC017792

Yi, G., Zhang, T., He, Y., Ye, H., Li, J., Bie, X., & Liu, D. (2020). Applicability analysis of four spatial interpolation methods for air temperature. JOURNAL OF CHENGDU UNIVERSITY OF TECHNOLOGY (Science & Technology Edition), 47(01), 115–128.

Yin, C., Yang, F., Wang, J., & Ye, Y. (2020). Spatiotemporal distribution and risk assessment of heatwaves based on apparent temperature in the One Belt and One Road Region. Remote Sensing, 12(7). Scopus. https://doi.org/10.3390/rs12071174

Zare, S., Hasheminejad, N., Shirvan, H. E., Hemmatjo, R., Sarebanzadeh, K., & Ahmadi, S. (2018). Comparing Universal Thermal Climate Index (UTCI) with selected thermal indices/environmental parameters during 12 months of the year. Weather and Climate Extremes, 19, 49–57. https://doi.org/10.1016/j.wace.2018.01.004

Zhan, L.-F., Wang, Y., Sun, H., Zhai, J., & Zhan, M. (2019). Study on the Change Characteristics of and Population Exposure to Heatwave Events on the North China Plain. Advances in Meteorology, 2019, e7069195. https://doi.org/10.1155/2019/7069195

Zhang, J., Yang, Z., Wu, L., & Yang, K. (2019). Summer high temperature extremes over Northeastern China predicted by spring soil moisture. Scientific Reports, 9(1), 12577. https://doi.org/10.1038/s41598-019-49053-9

Zhang, Y., You, Q., Mao, G., Chen, C., & Ye, Z. (2019). Short-term concurrent drought and heatwave frequency with 1.5 and 2.0 °C global warming in humid subtropical basins: A case study in the Gan River Basin, China. Climate Dynamics, 52(7), 4621–4641. https://doi.org/10.1007/s00382-018-4398-6

Zhao, M., Yu, J., & Hu, Y. (2021). Spatial interpolation of temperature in Chongqing area based on local thin-disk smooth spline function. Journal of Shaanxi Meteorology, 01, 50–55.

Zhao, Z., Huo, A., Zhang, D., Yi, X., Chen, S., Chen, S., & Chen, J. (2022). Assessing heat wave risk in Ningxia segment based on remote sensing. Arid Land Geography, 45(02), 512–521.

Zong, L., Liu, S., Yang, Y., Ren, G., Yu, M., Zhang, Y., & Li, Y. (2021). Synergistic Influence of Local Climate Zones and Wind Speeds on the Urban Heat Island and Heat Waves in the Megacity of Beijing, China. Frontiers in Earth Science, 9. https://www.frontiersin.org/article/10.3389/feart.2021.673786